Molecular dynamics simulations of $SrTiO_3$ thin-film growth from cluster deposition

J. Phys.: Condens. Matter **22** (2010) 045001 (9pp) doi:10.1088/0953-8984/22/4/045001

Molecular dynamics simulations of $SrTiO_3$ thin-film growth from cluster deposition

Jennifer L Wohlwend, Simon R Phillpot and Susan B Sinnott[1]

Department of Materials Science and Engineering, University of Florida, Gainesville, FL 32611, USA

E-mail: ssinn@mse.ufl.edu

Received 9 September 2009, in final form 20 October 2009
Published 5 January 2010
Online at stacks.iop.org/JPhysCM/22/045001

Abstract

We use classical molecular dynamics simulations to examine the deposition of $SrTiO_3$ stoichiometric clusters on (001) $SrTiO_3$. The simulations consider the deposition of clusters that consist of one, two, three or four stoichiometric units that have incident energies of 1.0 eV/atom. Two types of beam compositions are considered: those that are comprised of mono-sized clusters and those that are comprised of mixed-sized clusters along with individual SrO and TiO_2 particles. The results are analyzed to determine the effect of surface termination layer (SrO versus TiO_2), cluster size and beam composition on the resulting thin-film structure. The simulations indicate that termination layer and beam composition have an impact on the resulting film structure with mixed-beam composition and TiO_2 termination yielding films with a structure similar to that of bulk STO.

(Some figures in this article are in colour only in the electronic version)

1. Introduction

As the archetype perovskite, strontium titanate has been the subject of countless experimental and theoretical studies. $SrTiO_3$ (STO) possesses several properties that make it useful in electronic device applications; in particular, its high dielectric constant and low dielectric loss make it an attractive material in ferroelectric thin-film capacitors [1, 2], microwave applications [3], tunable resonant circuits [4] and dynamic random access memory applications [5]. Due to its lattice compatibility, STO is a desirable substrate material for high T_c superconductors; moreover, the growth of atomically smooth films on these substrates is critically important for the epitaxy and performance of heterostructures [6–9]. This has motivated an extensive examination of thin-film growth on STO.

The large Sr^{2+} cations are 12-fold-coordinated and sit on the corner sites while the smaller Ti^{4+} ions occupy all of the octahedral interstices surrounded by O^{2-} ions [10]. At room temperature, STO exists in the cubic paraelectric phase with a transition to the tetragonal antiferrodistortive phase at temperatures below its Curie point of 105 K [11] (110 K [12]).

Experimental work on the sputter deposition of TiO_2 thin films [13] indicated that TiO_2 clusters are present in the gaseous phase if the separation distance between the target material and the substrate is larger than the mean free path of the sputtered species (which is the average distance a particle travels before colliding with another particle). This separation distance gives the atomic species and small molecules in the gas phase time to combine and form clusters. The size of the clusters and subsequently deposited film were shown to be dependent on the target-to-substrate distance. In particular, a larger distance (250 mm) promoted the growth of larger clusters (30 Å in diameter) and yielded an amorphous TiO_2 thin film, whereas a shorter distance (50 mm) allowed only smaller clusters (less than 20 Å diameter) to form, thus producing a crystalline film. This illustrates the role of the type and size of the incident species on the morphology of the resulting films.

Molecular dynamics (MD) simulations were also carried out to elucidate the mechanisms associated with the deposition of Ti^{4+}, TiO^{2+}, TiO_2 and $Sr_4Ti_4O_{12}$ on STO [14]. When simulating the deposition of Ti^{4+}, TiO^{2+} and TiO_2, a corresponding vacancy was created within the substrate. This vacancy was then shown to be filled by the incident species but the deposition of several TiO_2 units was not considered. In the same work, the deposition of a two-unit STO cluster was considered to examine the homoepitaxial growth of STO. This cluster, however, had the unit cell geometry of bulk STO, thereby building the STO structure into the deposited film.

[1] Author to whom any correspondence should be addressed.

Table 1. Parameters used in the Buckingham and Coulombic potentials, from [24].

Interaction	A (eV)	ρ (Å)	C (eV Å^6)
$Sr^{1.331+}$–$O^{1.331-}$	139 621.961 934	0.1963	2.332 22
$Ti^{2.662+}$–$O^{1.331-}$	18 476.946 631	0.1963	0.0
$O^{1.331-}$–$O^{1.331-}$	21 943.289 277	0.2226	4.146 16

Cluster deposition has been extensively simulated for metals [15–18], where the effects of cluster size (from one to hundreds of thousands of atoms) and incident kinetic energy (from meV/cluster to MeV/cluster) has been investigated [19]. For example, Järvi *et al* utilized MD simulations to determine the effect of temperature on the maximum cluster size able to exhibit complete alignment between the cluster and the substrate and thus achieve epitaxy [18]. Small metallic clusters ($\leqslant$100 atoms/cluster) were found to become epitaxial from the energy released by initial impact due to melting and resolidification. In contrast, larger clusters (100–1000 atoms/cluster) required additional thermal energy to enable the diffusion of twin dislocations within the clusters, which was found to be the dominant mechanism responsible for attaining epitaxy.

The objective of this work is to use classical MD simulations to predict the morphology of STO thin films deposited on the (100) surface of STO. In particular, the effects of surface termination layer (SrO versus TiO_2), cluster size and size distribution are investigated. Our previous work elucidated the growth processes that occur during the deposition of SrO and TiO_2 thin films [20] as well as the deposition of SrO and TiO_2 monolayers [21] to create stoichiometric STO thin films. While monolayer deposition is analogous to molecular beam epitaxy, where elemental species are deposited, the deposition of clusters is comparable to pulsed-laser deposition (PLD) which involves the deposition of larger particles. The current simulations examine the atomic-scale processes that occur during the deposition of clusters containing 5–20 atoms. Our previous simulations [20, 21] indicated that there is little dependence of film structure on incident energy within the range studied (0.1–1.0 eV/atom). Surface termination, however, was found to have a significant effect on film structure with deposition upon TiO_2 termination yielding a more ordered film. Therefore, this work explores the influence of surface termination but considers only an incident energy of 1 eV/atom.

2. Computational details

Classical MD simulations are performed utilizing an empirical potential that describes atomic interactions. Electrostatic interactions are described by the Coulomb potential [22] and short-ranged interactions are modeled using the Buckingham potential [23], which represents the electron cloud repulsion and the attractive van der Waals contribution:

$$V_{\text{Buck}} = A_{ij}\exp\left(\frac{r_{ij}}{\rho_{ij}}\right) - \left(\frac{c_{ij}}{r_{ij}^6}\right). \tag{1}$$

Here, r_{ij} is the distance between any pair of atoms, i and j. The parameters A_{ij}, ρ_{ij} and C_{ij} are related to the ionic stiffness, radii and strength of the van der Waals interactions between ions, respectively. The potential parameters are obtained from Sekiguchi *et al* [24] and are given in table 1. Wunderlich *et al* [25] have compared the results with these parameters to those obtained with other parameter sets [26]; the current values were found to produce the smallest deviation from experimental structural properties. We compare the structural parameters determined using the current potential to the values obtained from DFT and experiment in table 2.

Previous computational surface energy calculations predict the SrO termination to be more favorable than the TiO_2 termination with surface energies of 1.37 eV and 1.33 eV, respectively, using the shell model [27] developed by Heifets *et al* [28]. Although our surface energy results predict SrO termination to be higher in energy than TiO_2 termination with calculated surface energies of 1.27 eV and 1.11 eV, respectively, the differences between the energies of the two surfaces are, in both cases, small. Moreover, our predictions are comparable to the average of the TiO_2 and SrO surface energies of 1.26 eV obtained using density functional theory (DFT) with the local density approximation [29]. As will be reported in a subsequent work, diffusion mechanisms and barriers calculated utilizing the current potential parameters and compared to barriers calculated with DFT yield comparable oxygen vacancy diffusion and ad-oxygen diffusion barriers. This collection of fiducial calculations gives us confidence that the potential used is suitably robust to examine thin-film growth. Long range forces can be further subdivided into electrostatic, induction and dispersion contributions. The electrostatic contribution is due to the permanent charge distribution while the other two encompass fluctuation charge contributions [23]. In this work these forces are represented by a Coulombic term (equation (2)):

$$V_{\text{Coul}} = \frac{1}{2}\sum_{i=1}^{N}\sum_{j\neq i=1}^{\infty}\left(\frac{q_i q_j}{r_{ij}}\right). \tag{2}$$

Here, q_i and q_j are the charges on atoms i and j, respectively, r_{ij} is the distance between them, and N is the total number of atoms.

It is well known that the pairwise r^{-1} sum in the Coulomb potential is conditionally convergent [22], meaning that in order for the potential to converge to zero there must be an infinite value for r_{ij}. This is not possible for the simulated system sizes; thus the potential requires special treatment. For this reason, the charged neutralized direct summation technique [30] is used:

$$V_{\text{Coul}} = \frac{1}{2}\sum_{i=1}^{N}\left(\sum_{\substack{j\neq i\\ r_{ij}<R_c}}\frac{q_i q_j}{r_{ij}} - \frac{q_i \Delta q_i(R_c)}{R_c}\right). \tag{3}$$

The first term is the $1/r$ pairwise potential while the second term is the Coulomb interaction of ion i with the neutralizing charge placed on the surface of the cutoff sphere of radius R_c, chosen here to be 10.148 Å. In these simulations, Newton's equations of motion are integrated using the Gear fifth-order predictor–corrector algorithm [31] with a time step of 1 fs.

Table 2. Comparison of calculated and experimental structure and elastic properties for STO.

	Present work	Previous computational work (DFT-LDA) [35]	Experimental
Lattice parameter (Å)	3.918	3.86	3.90 [36]
C_{11} (GPa)	405.18	421.0	317.2 [37]
C_{12} (GPa)	131.1	122.1	102.5 [37]
C_{44} (GPa)	131.1	133.2	123.5 [37]

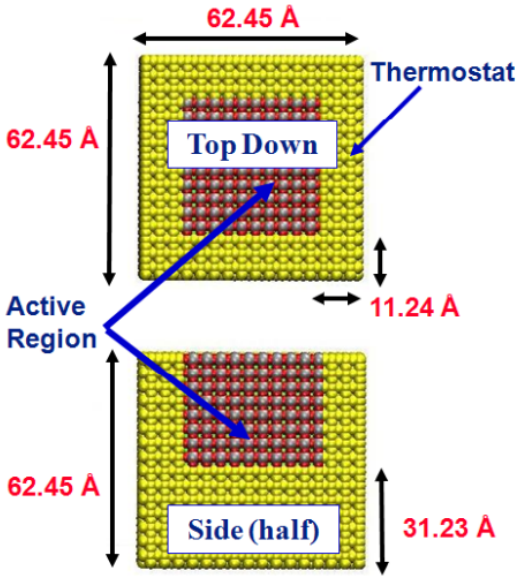

Figure 1. Arrangement of thermostat heat bath and dimensions of STO substrate.

The simulated system consists of two components: an STO substrate and a beam of incident particles. To model the substrate, a 16 × 16 × 16 cubic $SrTiO_3$ lattice is used that contains 20 480 atoms. The (100) free surface for deposition is simulated by leaving a ∼200 Å thick vacuum in the depositing [100] direction. To eliminate substrate size effects, periodic boundary conditions are imposed in the [010] and [001] directions. Prior to deposition, the system is ramped to 973 K in 100 K intervals and then equilibrated for 100 ps to ensure minimal energy fluctuations.

In a deposition experiment the kinetic energy of each incident particle is transferred to the atoms upon impact and is dissipated via phonon vibrations over the macroscopic-scale system. In the simulations, there is no such macroscopic region over which to dissipate the heat generated. Thus, in the absence of temperature control, this inevitably leads to an unphysical increase in the system temperature over time. Here, therefore, thermostat atoms are utilized in a heat bath arrangement (figure 1) to simulate energy dissipation, thereby better correlating to the experimental, macroscopic conditions. The thermostat involves rescaling the velocity of atoms at each time step so as to sustain a desired temperature. In addition to the temperature, the volume is also held constant during deposition such that the simulations are carried out in the canonical (*NVT*) ensemble. In other words, the system's thermodynamic state is described by a fixed volume, V, a fixed temperature and a fixed number of atoms, N.

Although examination of clusters of metals and some oxides are prevalent in the literature [17–19, 32–34], there is a lack of information on stoichiometric STO clusters. To create the clusters that are ultimately deposited, an STO crystal is cut into one-, two-, three- and four-unit stoichiometric STO clusters. To ensure the cluster geometry is comparable to that found in the plume created during PLD, the clusters are equilibrated in vacuum until minimal energy fluctuations are detected and the structure of the cluster stops changing.

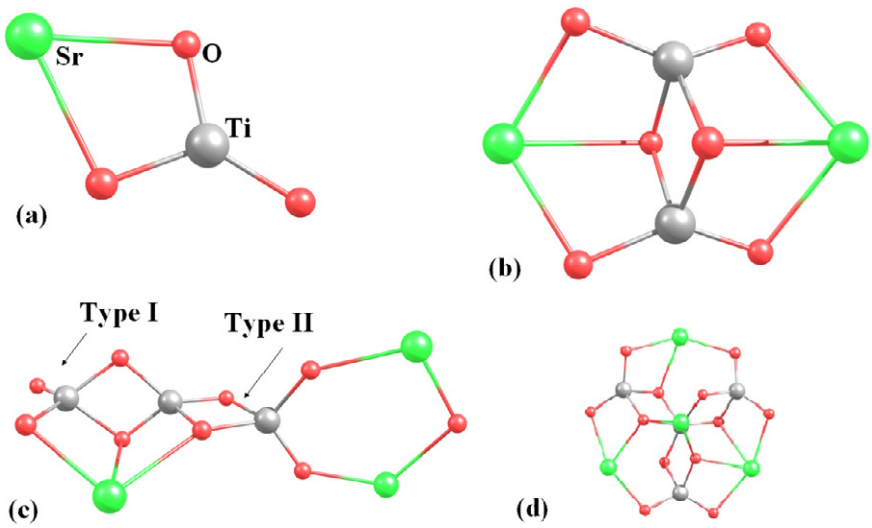

Figure 2. Stoichiometric STO clusters (a): one unit, (b): two units, (c): three units and (d): four units.

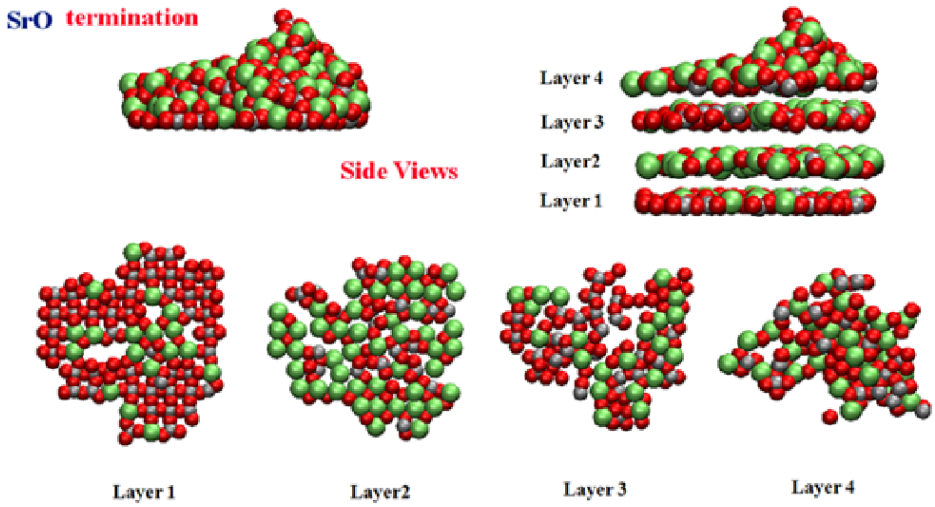

Figure 3. Representative snapshots of films deposited on SrO-terminated STO showing layer segregation and order within the first layer. Legend: Large, light atoms (green online): Sr; Small, light atoms (gray online): Ti; Small dark atoms (red online): O.

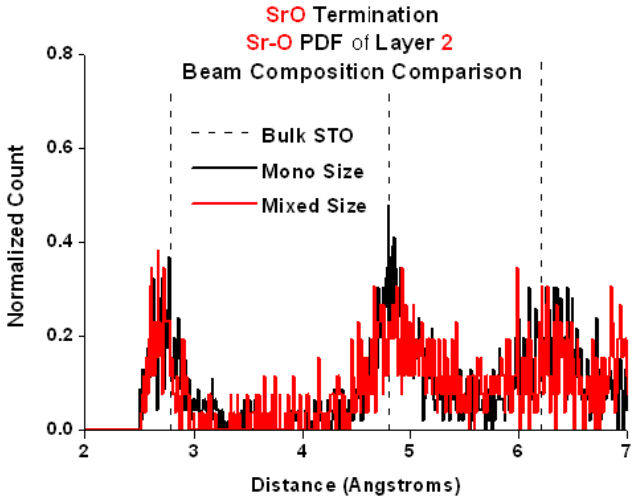

Figure 4. Pair distribution function (PDF) of the second deposited layer comparing mono- and mixed-size cluster deposition on SrO-terminated STO, illustrating the similar structural order between the two deposition methods.

Because the equilibrated clusters exhibit unique symmetry and surface-induced bond length variations, as illustrated in figure 2, this process reduces the bias associated with depositing clusters with the pre-existing STO crystal structure. The average Sr–O bond distance in all clusters is 2.6 Å compared to a bulk Sr–O distance of 2.77 Å. Clusters consisting of two or more STO units include two types of Ti–O bonds, Type I (1.9 Å) and Type II (1.7 Å) as indicated in figure 2, compared to the bulk Ti–O bond length of 1.95 Å.

For all deposition schemes examined, an incident kinetic energy of 1.0 eV/atom is allocated to each incident cluster by assigning a corresponding velocity to all the atoms within each cluster. The particles in the beam are deposited at random orientations and positions on the surface, with respect to their center of mass, and the distance between particles is varied to better understand the effect of deposition rate.

Table 3. Cluster deposition schemes investigated. Each scheme was performed on both terminations.

Deposition scheme		
Mono-sized Beam	Cluster size (STO units)	Separation distance (Å)
	1	30
	2	30
	3	20, 30, 60, 90 and 200
	4	30
Mixed-sized Beam	1–4 without SrO/TiO_2 particles	30 and 60
	1–4 with SrO/TiO_2 particles	30 and 60

The various scenarios examined are described in table 3 and consist of six unique deposition beams for each termination, resulting in a total of 12 unique systems. To analyze the effect of cluster size distribution, films are deposited by beams consisting of mono-sized clusters and by beams consisting of mixtures of one-, two-, three- and four-unit STO clusters along with SrO and TiO_2 particles in a random sequence. In addition to the unique beams, some systems are repeated, changing the distance between each deposition event, as indicated in table 3, to evaluate the impact of deposition rate. For three-unit STO clusters the vertical separation between incident depositing particles is varied from 20 to 90 Å and 200 Å, with the larger separation corresponding to a lower deposition rate. Furthermore, one- and four-unit STO mono-beam deposition and the mixed-beam depositions are repeated to investigate variations across different simulation trajectories for a total of five simulations each; no structural variance is found and the quantitative film composition analysis yields only a 4–18% variance between the repeated simulations on the TiO_2 termination and 8–25% variance between repeated simulations on the SrO termination. After depositing approximately 200 atoms (40 one-unit STO, 20 two-unit STO, 15 three-unit STO, and 5 four-unit STO

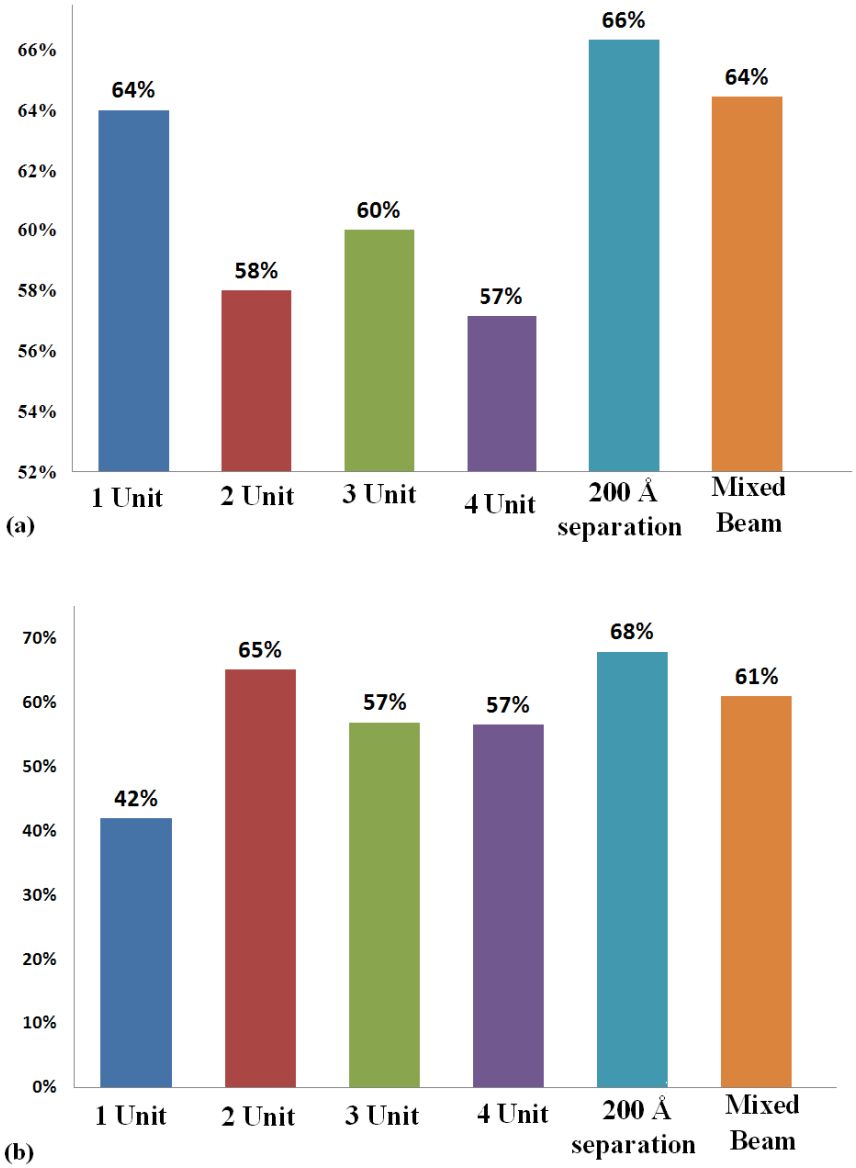

Figure 5. Percentage of metal atoms in the first two deposited layers on SrO-terminated STO: (a) Ti atoms in first layer, (b) Sr atoms in second layer.

clusters) the system is allowed to equilibrate at an elevated temperature of 1100 K for approximately 50 ps. After approximately 100 STO units are deposited, corresponding to four ML (two SrO and two TiO_2), the system temperature is ramped to 2000 K, held for 300 ps to allow further structural equilibration, and then for analysis purposes quenched to 0 K to eliminate thermal effects.

3. Results

Various analysis methods are used to both qualitatively and quantitatively describe the deposited thin films. First, layer-by-layer snapshots of the films illustrate the structural order and are compared to the layering sequence in bulk STO. The percentages of metal atoms present in each layer are also calculated as an indication of mixing within each layer, and to characterize the possible dependence of layer composition on the differing deposition schemes. This analysis compares the layering present within the film to the alternating SrO/TiO_2 planes present in bulk STO. For example, the first deposited layer on SrO termination should have predominantly Ti cations whereas the first layer on TiO_2 termination should contain Sr cations. To quantitatively analyze the structural order of the deposited films, pair distribution functions (PDFs) are calculated for each deposited layer. The Ti–O PDF, for example, characterizes the nearest-neighbor distances of Ti within each film with surrounding O atoms.

For all film depositions, the first deposited layer produces PDFs consistent with bulk STO, meaning they have the same Sr–O and Ti–O neighbor distances as the corresponding SrO and TiO_2 planes in STO. The second deposited layer, however, shows deviation from bulk-like structure. Therefore, the PDFs for the second deposited layer for all schemes investigated are analyzed and discussed.

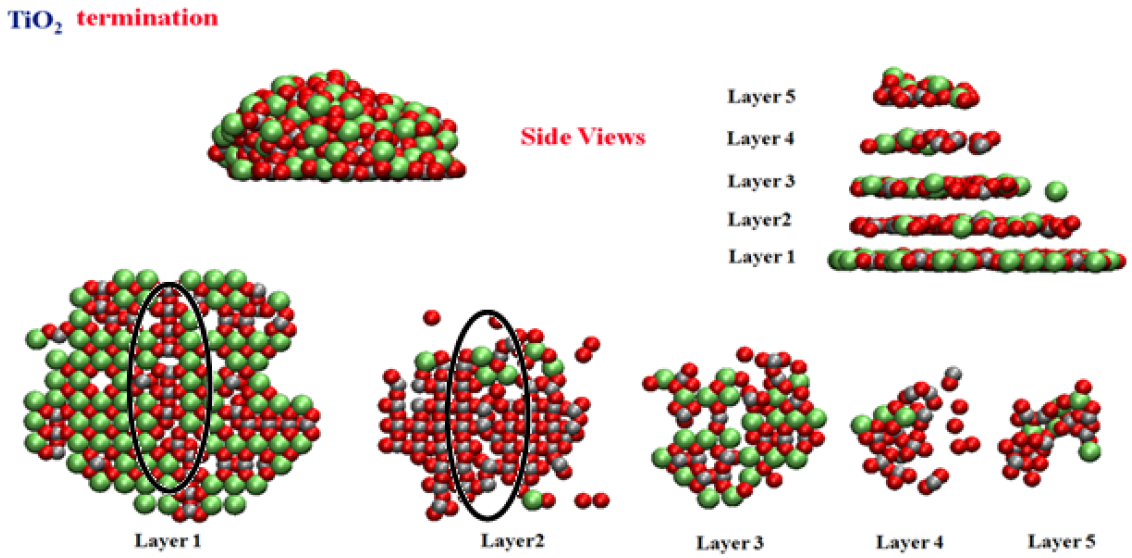

Figure 6. Representative snapshots of films deposited on TiO_2-terminated STO showing layer segregation and order within layers 1 and 2 shown in the lower figures. The circled areas depict the effect of first layer TiO_2 inclusions on the subsequently deposited second layer. Color scheme the same as in figure 3.

STO thin films deposited on the SrO termination produce similar morphologies for each scheme; representative snapshots are shown in figure 3 with each atomic layer separated for visual inspection. Each layer is approximately 2 Å thick, corresponding to half the lattice parameter. It is noted that the fourth 'layer' appears thicker than the previous layers. This is due to the breakdown of strict crystalline layering in the film; therefore analysis is performed on the multiple-layer-thick top portion. Figure 3 shows areas of TiO_2 ordering separated by SrO molecules in the first layer, with no visually apparent order in the second layer. PDFs are constructed and compared for all of the processing variables studied: cluster size, deposition rate and size distribution. A representative PDF of the second deposited layer comparing two different deposition schemes, mono-sized and mixed-sized deposition, is shown in figure 4 illustrating similar peak positions for both schemes. Films deposited by all schemes on SrO-terminated STO have similar peaks to the Sr–O layer in bulk STO up to the second nearest neighbor, damping out significantly afterward. Metal atom percentages, given in figure 5, also indicate no systematic dependence on the deposition scheme, with a 9% spread in Ti atom percentage within the first layer (figure 5(a)) and a 26% spread of Sr atom percentage in the second deposited layer (figure 5(b)).

Next, we examine films deposited on the TiO_2 termination. A representative snapshot of such a film is given in figure 6 where the layers are again separated to illustrate the ordering and composition of each layer. Representative Ti–O PDFs for films produced from mono-sized versus mixed-sized beams shown in figure 7 display similar peak positions, height and width for each scheme. The Ti–O peaks describing the second layer are the same as those representing the TiO_2 plane in bulk STO.

Metal atom percentages within the first two layers are given in figure 8. The percent of Sr atoms in the first layer

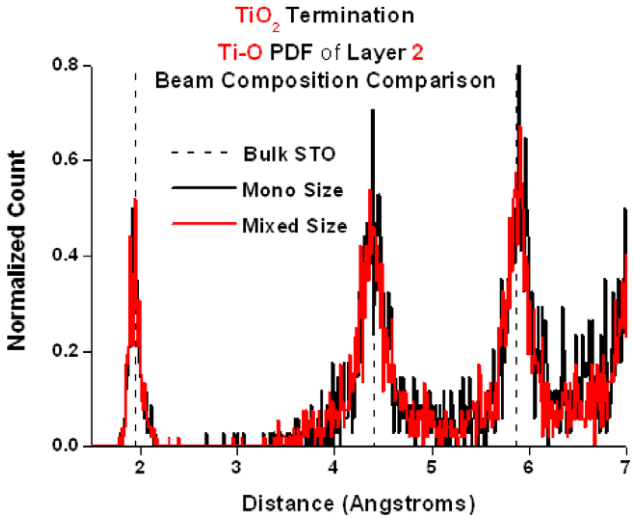

Figure 7. PDF of the second deposited layer, comparing mono- and mixed-size cluster deposition on TiO_2-terminated STO illustrating the similar structural order between the two deposition methods.

and Ti atoms in the second layer varies by 20% between the deposition schemes, with mixed-beam deposition having the highest percentage of expected metal atoms for both layers.

Further inspection of the snapshots of the first deposited layer of each film on TiO_2-terminated STO (figure 9) identifies the most prevalent defects observed as fourfold site vacancies, Ti antisites and TiO_2 inclusions, as indicated in figure 10(a). To evaluate the impact of the deposition scheme on the defects described in figure 10(a), the percentage of the overall defects present compared to the total fourfold sites available is calculated and shown in figure 10(b). Taking all defects into consideration within the first deposited layer is an indication of its structural quality and can affect the second deposited layer. This is shown in the circled areas in figure 6 where

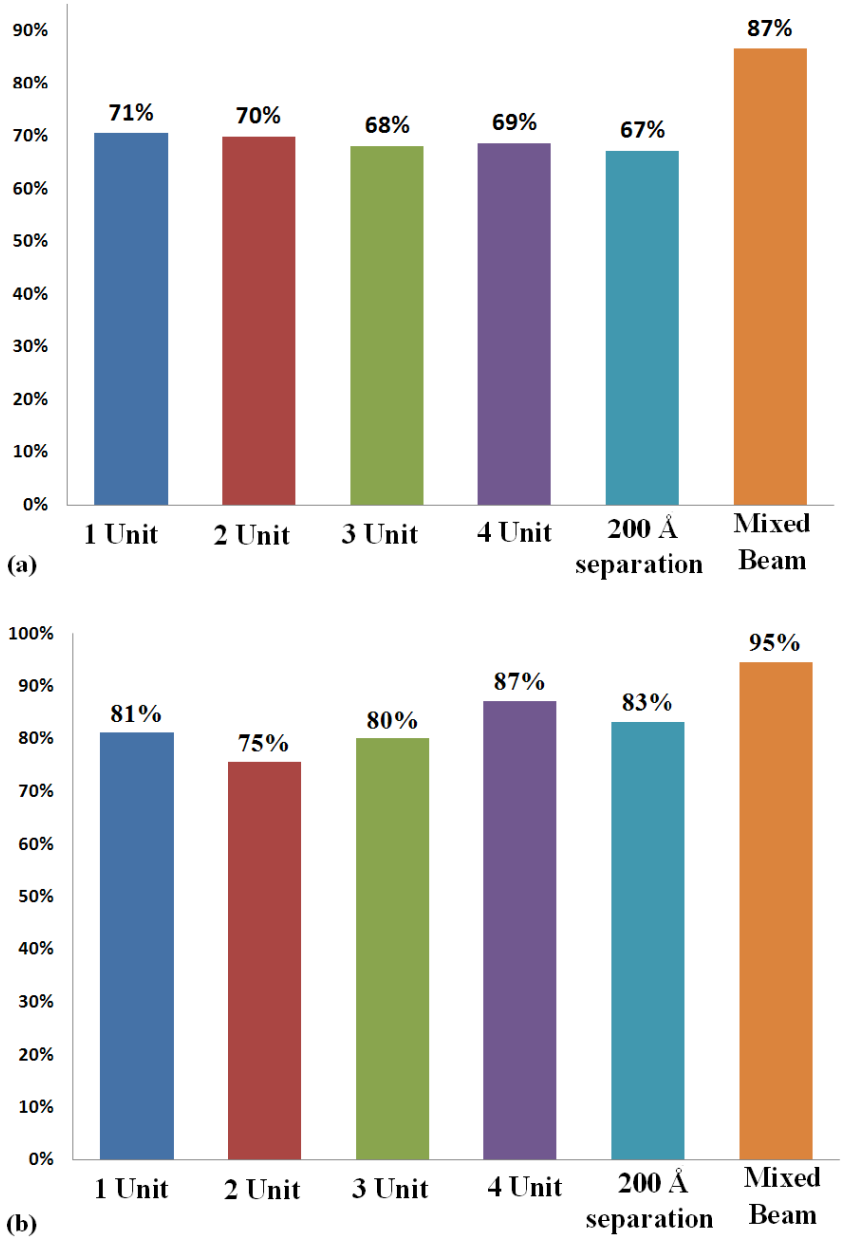

Figure 8. Percentages of metal atoms in the first two deposited layers on TiO_2-terminated STO. (a) Sr atoms in first layer and (b) Ti atoms in second layer.

the TiO_2 inclusions create regions of disorder in the second layer. Films deposited from mixed-sized beams have the lowest overall number of defects present in the first layer.

4. Discussion

Films deposited on SrO-terminated STO for all schemes investigated yield a partially ordered first layer with very little structural order in the second layer or beyond. No dependence on cluster size distribution or deposition rate is predicted. The overall film structure on the TiO_2 termination can be described as having regions of order similar to that in bulk STO, but with three structural defects: Ti antisites on Sr sites, TiO_2 inclusions, and fourfold site vacancies. The first deposited layer on both terminations has a degree of structural order comparable to bulk STO, as evidenced by the percentage of metal atoms within the layer and the PDFs. STO films deposited on TiO_2-terminated STO, however, manifest two ordered (or semi-ordered) layers before its structural order deteriorates to fully disordered layers, Films deposited on SrO-terminated STO, by contrast, only retain structural order in the first deposited layer. The PDFs also indicate that films deposited on the SrO termination only exhibit order up to the second-nearest neighbor, whereas the PDFs for the films deposited on the TiO_2 termination exhibit longer-ranged order.

Comparing the metal atom percentages for the two terminations indicates that films deposited on the TiO_2 termination have an overall higher percentage of expected metal atoms within each layer compared to films deposited on SrO-terminated STO. There is not a clear effect of

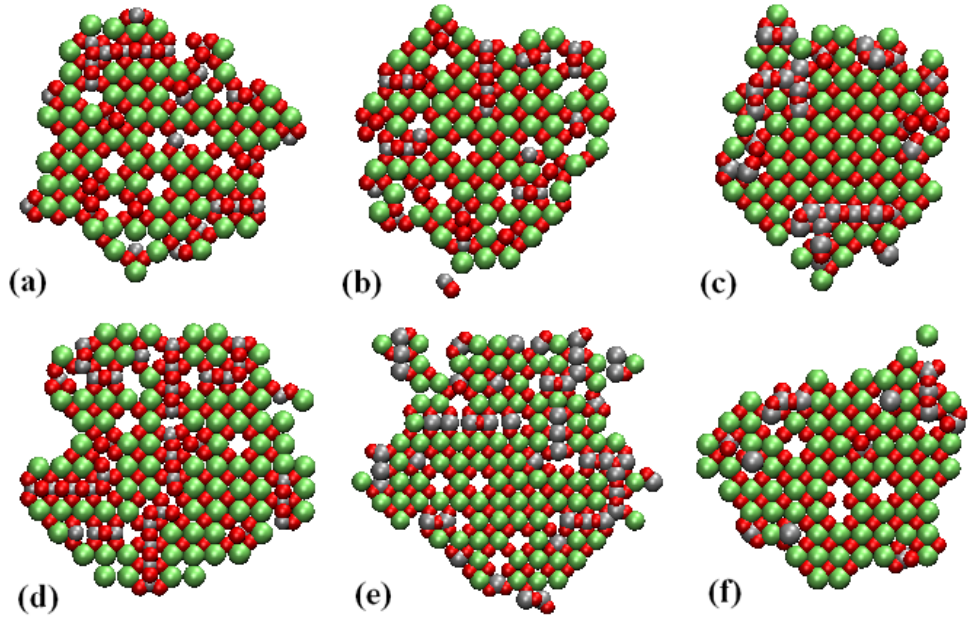

Figure 9. First layer of each film deposited on TiO_2 termination displaying fourfold site vacancies, TiO_2 inclusions and Ti antisites (for structural details see figure 10 b). (a) 1-unit STO, (b) 2-unit STO, (c) 3-unit STO, (d) 4-unit STO, (e) 3-unit STO with 200 Å separation, (f) mixed-size distribution beam with SrO and TiO_2 particles. Color scheme the same as in figure 3.

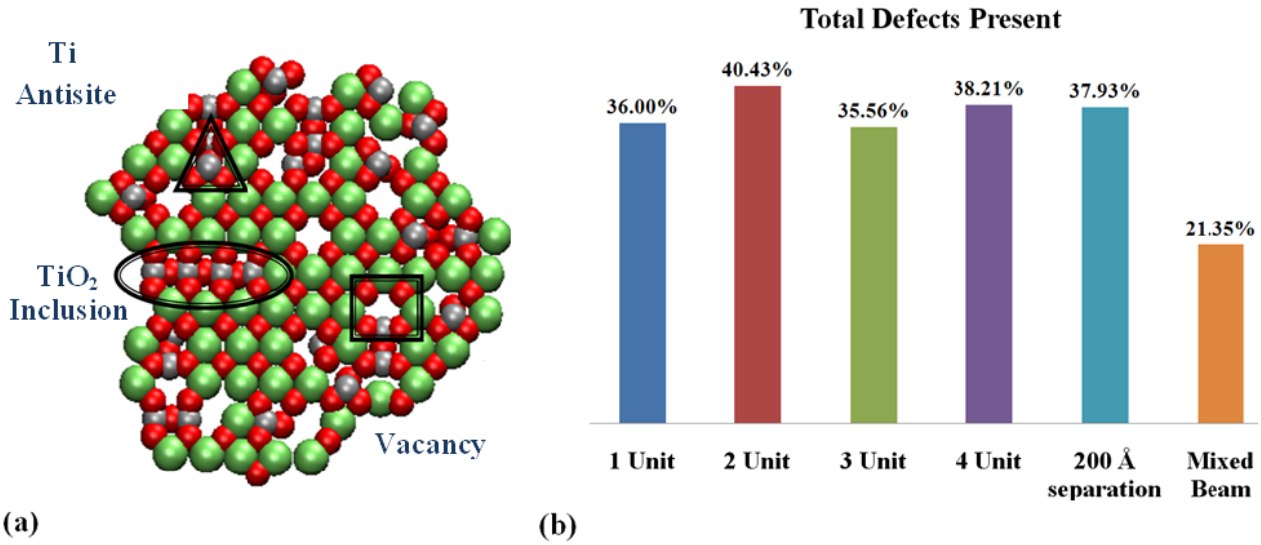

Figure 10. (a) Defects present in deposited films on TiO_2 termination. Triangle: Ti antisite; oval: TiO_2 inclusion; square: fourfold vacancy. (b) Overall percentages of defects present in the first deposited layer. Color scheme the same as in figure 3.

the deposition scheme on layer composition since the differences are within the statistical variance between repeated simulations. The PDFs comparing mono-and mixed-beam deposition show the same peak position and width, also indicating that the various schemes have minimal effect on the deposited film structure. Looking at the defects observed within the first deposited layer, the Ti antisite is the most prevalent defect for the one-unit STO beam, while TiO_2 inclusions dominate with a four-unit STO beam. Also looking at the defect percentages, it appears that TiO_2 inclusions increase with increasing cluster size; however, there is no apparent trend for the occurrence of Ti antisites. Fourfold site vacancies are also an indication of the planar density of the deposited films. Cluster size and deposition rate, over the ranges considered, display no apparent influence on vacancies; however, the mixed-beam deposition including SrO/TiO_2 particles contains fewer vacancies compared to the mixed-beam deposition without these particles.

5. Conclusions

Analyzing the effects of incident particle size is accomplished by the deposition of stoichiometric clusters of differing sizes. To determine the effect of the cluster size distribution within

the beam, films are also grown by depositing beams comprised of one- to four-unit STO clusters with and without SrO and TiO_2 particles. It is apparent that TiO_2-terminated STO yields films with ordered first and second layers while the SrO termination only has an ordered first deposited layer. Defects in the first layer deposited on the TiO_2 termination shows a slight dependence on deposition scheme with the mixed-sized beam including SrO/TiO_2 particles having the lower overall number of defects present when compared to both mixed-size beams without SrO/TiO_2 and mono-sized beams. The analysis of the deposited films leads to the conclusion that cluster size and deposition rate, within the range studied, has no effect on the structure of the deposited film. The termination effect is shown to impact the resulting film structure, as was seen in the previous deposition studies where films deposited on TiO_2-terminated STO exhibit a more highly ordered film as compared to SrO-terminated STO.

Acknowledgment

This work was supported by the National Science Foundation under DMR-0426870.

References

[1] Zhou C and Newns D M 1997 *J. Appl. Phys.* **82** 3081
[2] Rinaldi F 2002 Basics of molecular beam epitaxy (MBE), Optoelectronics Department, University of Ulm, p 1
[3] Petrov P and Carlsson E F 1998 *J. Appl. Phys.* **84** 3134
[4] Treece R E, Thompson J B, Mueller C H, Riykin T and Cromar M W 1997 *IEEE Trans. Appl. Supercond.* **7** 2363
[5] Roy D, Peng C J and Krupanidhi S B 1992 *Appl. Phys. Lett.* **60** 2478
[6] Tsuchiya R, Kawasaki M, Kubota H, Nishino J, Sato H, Akoh H and Koinuma H 1997 *Appl. Phys. Lett.* **71** 1570
[7] Heifets E, Eglitis R I, Kotomin E A, Maier J and Borstel G 2002 *Surf. Sci.* **513** 211
[8] Nakamura T, Inada H and Iiyama M 1998 *Appl. Surf. Sci.* **130–132** 576
[9] Schrott A G, Misewich J A, Copel M, Abraham D W and Zhang Y 2001 *Appl. Phys. Lett.* **79** 1786
[10] Moulson A J and Herbert J M (ed) 2003 *Electroceramics: Materials, Properties, Applications* (New York: Wiley)
[11] Vanderbilt D 1997 *Curr. Opin. Solid State Mater. Sci.* **2** 701
[12] Shirane G and Yamada Y 1969 *Phys. Rev.* **177** 858
[13] Barnes M C, Gerson A R, Kumar S and Hwang N-M 2004 *Thin Solid Films* **446** 29
[14] Miyamoto A, Takeichi K, Hattori T, Kubo M and Inui T 1992 *Japan. J. Appl. Phys.* **31** 4463
[15] Tochitsky E I, Gritskevich R N and Obukhov V E 1985 *Thin Solid Films* **131** 289
[16] Bönnemann H and Nagabhushana K S 2007 Metal nanoclusters: synthesis and strategies for their size-control *Metal Nanoclusters in Catalysis and Materials Science: the Issue of Size Control* ed B Corain, G Schmid and N Toshima (Amsterdam: Elsevier) p 21
[17] Hendy S C and Hall B D 2001 *Phys. Rev.* B **64** 085425
[18] Jarvi T T, Kuronen A, Meinander K, Nordlund K and Albe K 2007 *Phys. Rev.* B **75** 115422
[19] Nordlund K, Jarvi T T, Meinander K and Samela J 2008 *Appl. Phys.* A **91** 561
[20] Wohlwend J L, Behera R K, Jang I, Phillpot S R and Sinnott S B 2009 *Surf. Sci.* **603** 873
[21] Wohlwend J L, Boswell C N, Phillpot S R and Sinnott S B 2009 *J. Mater. Res.* **24** 1994
[22] Allen M P and Tildesley D J 1987 *Computer Simulation of Liquids* (New York: Oxford University Press)
[23] Buckingham A D 1975 *Phil. Trans. R. Soc.* B **272** 5
[24] Sekiguchi S, Fujimoto M, Nomura M, Cho S-B, Tanaka J, Nishihara T, Kang M-G and Park H-H 1998 *Solid State Ion.* **108** 73
[25] Wunderlich W, Fujimoto M and Ohsato H 2000 *Thin Solid Films* **375** 9
[26] Katsumata T, Inaguma Y, Itoh M and Kawamura K 1998 *Solid State Ion.* **108** 175
[27] Borstel G, Eglitis R I, Kotomin E A and Heifets E 2002 *J. Cryst. Growth* **237–239** 687
[28] Heifets E, Kotomin E A and Maier J 2000 *Surf. Sci.* **462** 19
[29] Padilla J and Vanderbilt D 1998 *Surf. Sci.* **418** 64
[30] Wolf D, Keblinski P, Phillpot S R and Eggebrecht J 1999 *J. Chem. Phys.* **110** 8254
[31] Sutmann G 2002 *Quantum Simulations of Complex Many-Body Systems: From Theory to Algorithms* ed J Grotendorst, D Marx and A Muramatsu (Julich: John von Neumann Institute for Computing) p 211
[32] Giglio E, Reinhard P-G and Suraud E 2000 *J. Phys. B: At. Mol. Opt. Phys.* **33** L333
[33] Tanaka N, Peng D L, Sumiyama K and Hihara T 2008 *Thin Solid Films* **516** 1677
[34] Li Y, Blaisten-Barojas E and Papaconstantopoulos D A 1998 *Phys. Rev.* B **57** 15519
[35] Piskunov S, Heifets E, Eglitis R I and Borstel G 2004 *Comput. Mater. Sci.* **29** 165
[36] Abramov Y A, Tsirelson V G, Zavodnik V E, Ivanov S A and Brown I D 1995 *Acta Crystallogr.* B **51** 942
[37] Bell R O and Rupprecht G 1963 *Phys. Rev.* **129** 90